Sigma Journal of Engineering and Natural Sciences
Web page info: https://sigma.yildiz.edu.tr
DOI: 10.14744/sigma.2022.00038

Research Article

A computational fluid dynamics-discrete element modeling study on flow field and particle sedimentation processes in a disk-stack centrifuge settler

Orçun EKIN*[1], Yunus ÇERÇI[1]

[1]*Department of Mechanical Engineering, Faculty of Engineering, Adnan Menderes University, Aydın, 09000, Turkey*

ARTICLE INFO

Article history
Received: 01 December 2021
Accepted: 10 July 2021

Key words:
CFD-DEM; Disk-stack Centrifuges; Particle-laden Flows

ABSTRACT

One aspect of centrifugal disk settlers comes forward when assessing the sedimentation capability of a unit separation volume, i.e., a single disk interval. Although laboratory analyses of discharged effluent give an approximation as to sediment radii and quantity in unit volume, the fraction of sedimentation at different process parameters such as disk angular velocity, particle diameters of interest, throughput rates etc. stand obscure. Towards revealing how centrifugal forces act on the sedimentation process alongside the settler geometry and fluid-particle characteristics, a CFD-DEM model of flow field between two adjacent disks at an arbitrary position in disk-stack is presented in this study. Simulations, comprised of particular sediment diameters are conducted at different angular velocities, hence centrifugal forces. Particle sedimentation percentages, also trajectories of each injected particle in different categories are extracted and summarized with an insight on pressure and velocity distributions in the flow field.

Cite this article as: Ekin O, Çerçi Y. A computational fluid dynamics-discrete element modeling study on flow field and particle sedimentation processes in a disk-stack centrifuge settler. Sigma J Eng Nat Sci 2022;40(2):344–357.

INTRODUCTION

Centrifugal separators are utilized in many branches of industry where particle or phase extraction from a multiphase-multicomponent fluid system is required, such as mining and mineral processing, chemical processes, oilfield applications, beverage and dairy products and waste water treatment. As the driving force in passive sedimentation is gravity, centrifugal settlers conduct the settling of particles or phases of immiscible fluids by centrifugal force. The versatility of gravitational or centrifugal settling comes from the idea that different densities of contributing phases of fluid, in the presence of gravity of centrifugation, will create different mass forces, resulting in proper separation

***Corresponding author.**
*E-mail address: orcun.ekin@adu.edu.tr

This paper was recommended for publication in revised form by Mostafa Safdari Shadloo

of phases and/or particles. Different geometric features of disks or interiors, throughput rates and centrifugal forces can be implemented for different separation tasks as possible fields of applications are growing larger continuously. Although centrifugal sedimentation can be performed in a variety of devices, such as decanter centrifuge and solid-bowl centrifuge [1], the disk-stack centrifuge is considered to be the most complicated and powerful example of a centrifugal settler which allows extreme g-forces and separation performance, therefore satisfying the increasing industrial demand for finer and finer extraction of phases.

In centrifugal separator operation, the mixture is introduced into the separation volume (i.e. 'bowl') through a stationary tube, i.e. feed pipe (Fig. 1). The bowl rotates around the axis of feed pipe at a constant rate, the value of which is mainly determined by the fluid and particle characteristics of medium, like particle volume percentage, fluid density and dynamic viscosity, etc. [2]. The number of disks (hence, the number of channels) is determined in a way that the available vertical gap between the distributor and bowl conical part is completely filled up with disks. This way, the alternative routes of fluid where sedimentation where the disk-stack is by-passed can be prevented. When introduced from the inner radius of disk interval, the solid particles incline through the downward slope of conical channel due to density difference and leave the settling volume from the outer radius. A clarifying centrifuge principally concentrates microorganisms in milk structure

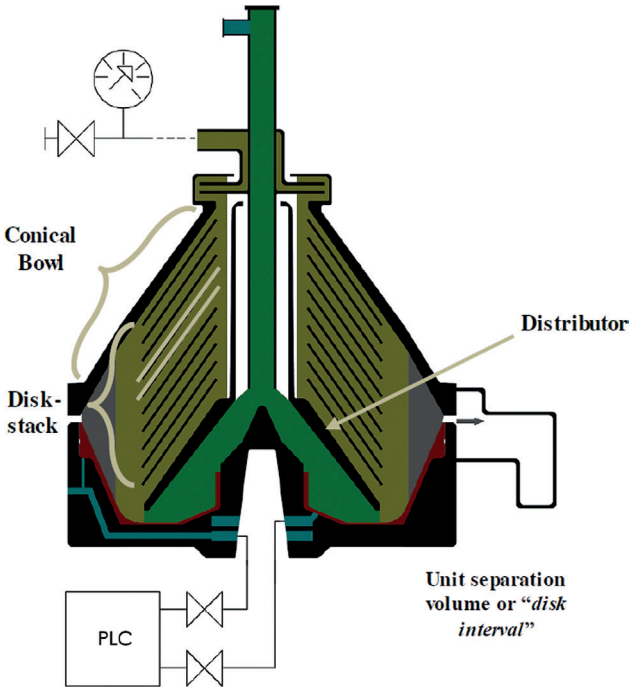

Figure 1. Full cross-section view of a typical 2-phase centrifugal disk separator and unit separation volume.

on the periphery of the bowl due to their higher density relative to continuous fluid. A small amount of milk enriched with microorganisms (centrifugate) is extracted from the bowl at intervals in drop-bottom bowls or continuously as in nozzle-separators [3].

In this study, the disk interval to be investigated is extracted from the mid-section of disk-stack. Representing a singular flow channel in which the sedimentation process takes place, the CFD-DEM investigation of this domain has the promise of characterizing and benchmarking the different process parameters that have the ability to affect the outcome, that is the sedimentation performance. However, when the previous studies in the literature considered, a CFD approach is not a novelty. In fact, Leung [4] offered a set of simulations to describe the conditions and flow character through the disk-stack and the rest of the fluid volume inside a centrifugal separator and the mammalian cell separation in a disk-stack centrifuge via CFD by Euler-Euler coupling particle laden flow representation was also investigated in different studies [5, 6]. However, the current study outstands in both problem definition and applied methods when compared to the earlier literature. Through this implementation of the problem; particle sedimentation behavior due to geometric features and flow properties through a channel comprised of two adjacent disks can be now explained by the help of an effective discrete particle tracking structure, that is Eulerian-Lagrangian Coupling [7]. The outright assumption that the flow is distributed evenly between the disks comprising the disk-stack [8] is also avoided by applying a preliminary model specifically built and validated for this purpose in a previous study [9]. This model is utilized to provide the velocity inputs on the inlet boundary of channel geometry, an information which otherwise cannot be harvested conveniently by traditional methods of flow measurement, given the intricate character of a disk-stack centrifuge [10].

PROBLEM DEFINITION

The unit flow field in a disk-stack centrifuge is a domain generated by two subsequent disks in the disk-stack. This definition is abbreviated to 'single disk interval'. The two-phase fluid is forced to flow upwards and through the interval as the outlet is located at a diameter, smaller than that of disk outer radius, where the inlet boundary is. The disk interval is inclined 35° with inner and outer radii of 45mm and 82mm, respectively (Fig. 2). The density of bovine milk, the continuous medium in this study has a range between 1.027 and 1.035 g/cm^3 at 20°C, while its viscosity is approx. 0.003 Pa.s at the same temperature [11].

To offer a proper insight to the particle settling behavior of the current disk structure, cut-off [8] particles corresponding to 3 different diameters are simulated. These particles, with diameters 2.086μm, 3.131μm and 6.259μm (see Table 1) are then introduced into the disk interval in

separate injections. A secondary set of runs to investigate the response of particles above and below the cut-off sizes under given conditions is conducted via injecting particles at an interval of 0.01μm and 12μm. Constant-diameter injections are preferred over distribution methods such as Rosin-Rammler [12] in order to properly control the number of elements and diameters to be tracked at every turn of simulation.

Three different bowl speeds are considered to observe particle discharge time and sedimentation ratio dependencies on speed. Here, the original centrifugal separator on which the previous studies were conducted has a nominal bowl rate of 7,700rpm. The remaining two angular rates of 3,850rpm and 11,550rpm are determined simply by halving and doubling this nominal rate, respectively. This range, in actual machines, is much narrower since the target particle (in this case somatic cells) seldom displays a wide spread in terms of diameters. The bowl (hence, channel) rates in this study are selected so that the change in sedimentation character with varying angular velocity (hence, g-force) may provide significant results, drawing a limit to the extremes of a very specific procedure. The velocities at which the particles are introduced into the separation domain are calculated based on the 3D model where a quarter-section of the actual machine is adopted. As seen on Fig. 3, the velocities are averaged at the inlet boundaries throughout the machine using a set of revolved surfaces [9].

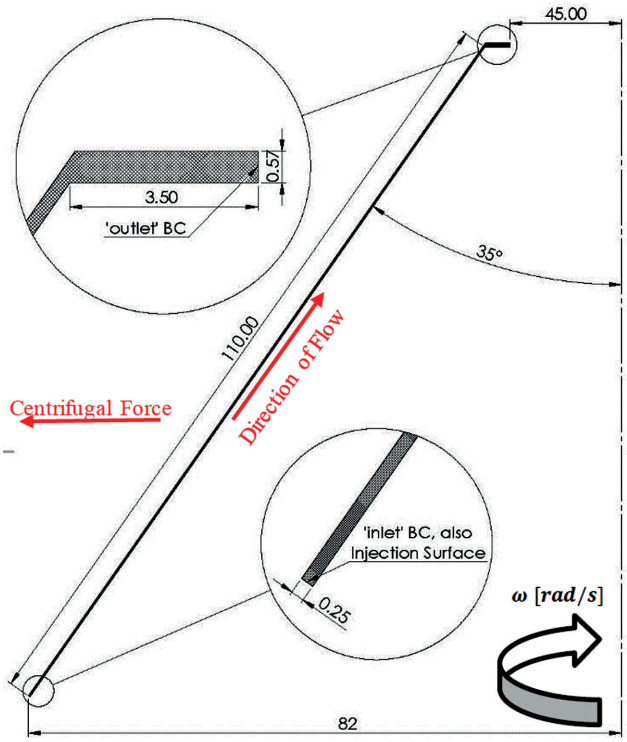

Figure 2. Full cross-section view of a typical 2-phase centrifugal disk separator and unit separation volume.

Somatic cells can be explained as a collection of milk-producing cells (about 2%) and cells coming from the immune system (the other 98%). In this study, a specific type of somatic cells, leukocytes (i.e. white blood cells, from the immune system) are investigated in terms of their sedimentation behavior. As the excessive amounts of leukocytes per ml of milk deteriorate the texture, odor, taste and shelf life of the substance, allowed thresholds for milk acceptance in dairy industries are applied depending on the legal regulation of countries; e.g., the values for bovine milk in Germany, Canada, and the USA are 1×10^5, 5×10^5, and 7.5×10^5 cells/mL, respectively [13].

In the context of this study, the leukocyte physical properties and their characteristics in bovine milk specimens are translated into the Computational Fluid Dynamics - Discrete Element Modeling (CFD-DEM) environment for settling behavior inspection. The values for the two critical parameters of leukocyte particles in terms of computational

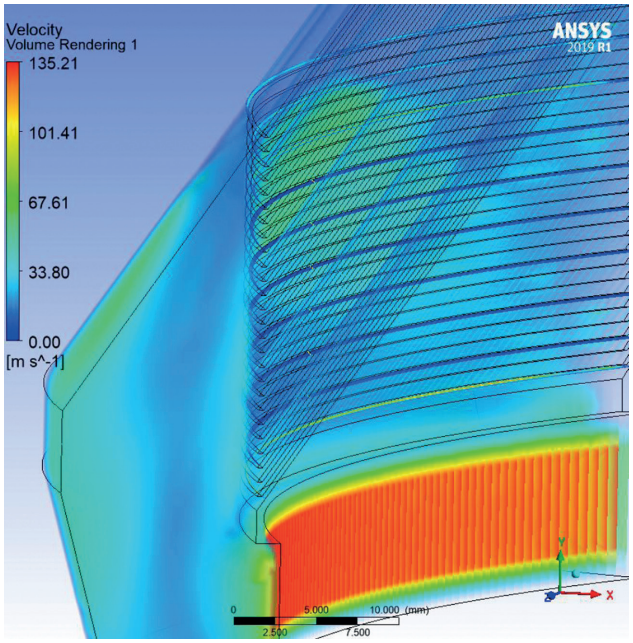

Figure 3. Channel inlet velocities are determined via sampling from revolved surfaces from a large-scale model (representation: 7700rpm bowl angular velocity).

Table 1. Cut-off particle diameters for increasing bowl rates.

Bowl Rate [rpm]	Inlet Velocity [m/s]	Critical Diameter [μm]
3850	1.858	6.259 μm
7700	3.629	3.131 μm
11550	5.531	2.086 μm

methods, i.e. particle density and cell diameters are adopted from prior publications in this field [14, 15]. Based on these parameters, particle settling behavior of a specific configuration of the specified flow field is investigated via CFD-DEM mainframe.

METHODOLOGY

Cleaning or refining the phases in centrifugal separators is a reliable and -to a certain extent measurable procedure, yet complicated machine structures and operating principle prohibit an in-depth investigation based on experiment and real-time monitoring. The mathematical prediction on how a centrifugal separator will operate with prescribed geometrical and throughput parameters, is defined through a cut-off size, that is, the largest particle in effluent, and the smallest in sludge [8]. These predictions assume no fluid-particle interaction (in a way that particles affect the turbulence characteristics of fluid), certain flow patterns, steady conditions and 2D simplification of actual flow domain. Although when utilized properly, "cut-off size" appears to be sufficient to give an insight on separation capability of a certain machine, both for designing and scaling-up purposes and has been utilized in the industry for decades. With minute differences are available between the methods to determine the separation ability of a certain centrifuge, the Stokes' velocity (Eqn. 1) applies to these approaches conveniently [10]:

$$\vartheta = \frac{g d_p^2 (\rho_p - \rho_m)}{18\mu} \quad [m/s] \tag{1}$$

where 'g' is the gravitational acceleration of the earth, μ is the dynamic viscosity of the continuous fluid (bovine milk, in this study) and (ρ_p-ρ_m) is the difference between the particle and the medium densities, respectively. Stokes' Law simply states that the sedimentation velocity ϑ is determined by the particle diameter, difference between the particle and medium densities and inevitably the dynamic viscosity of the medium. Density difference is proportional to the settling velocity, while the diameter of the particle is related by its square. As seen from the Eqn. 1, if the fluid and particle densities are by nature equal, the particle is suspended in the presence of gravitational forces. Also, an increase in dynamic viscosity increases the rate at which the particle is sedimented, or for a constant settling velocity, now a larger diameter particle can be sedimented, which is a typical trade-off when scaling-up a centrifuge settler.

The Relative Centrifugal Force (RCF) in centrifugal separation applications simply replaces the earth's gravitational field to control the primary operation parameters i.e. settling rate and critical (cut-off) particle. The RCF the continuous medium is exposed to is calculated via Eqn. 2;

$$RCF = \frac{\omega^2 r}{9.81} \quad [m/s^2] \tag{2}$$

where r is the particle's distance to axis of rotation; ω is the angular velocity of the centrifuge which can be calculated from the Eqn. 3 (where N represents the rotor rate, in rpm):

$$\omega = N\frac{2\pi}{60} = N \times 0.10472 \quad [rad/s] \tag{3}$$

Relative centrifugal force expression in Eqn. 2 is simply replaced with the gravitational force of the earth in the Stokes' Law to yield the theoretical minimum diameter calculation utilized to assess centrifuge performance of particle sedimentation.

As ever-increasing computational resources coming at reasonable costs, the CFD has become an integral part of investigating intricate problems on fluid flow phenomena encountered in modern industry, thus separation of multiphase-multicomponent flows. The DEM was first introduced by Cundall and Strack [16] to model granular flows and has become a widely accepted and efficient way of modeling of such applications. Tsuji, Kawaguchi and Tanaka et al. [17] first proposed a DEM algorithm coupled to traditional CFD with prospect applications in fluidized beds and particulate gas flows. Based on this approach, significant advancement has been established in the field of particulate multiphase flows with varying features in problem definitions and boundary conditions.

Model Description

CFD-DEM is one of the several approaches available to model multiphase, multi-component flow systems. Alternative modeling and solution methods are summarized elsewhere [18, 19]. Two of the prominent examples of these variety of methods are Euler-Euler and Euler-Lagrange schemes. In the Euler-Euler scheme (fluid-fluid scheme), the two components of fluid present a miscible continuum [20]. However, the discrete characteristics of a solid phase (sediment, contaminant etc.) cannot be described in the Euler-Euler method [21]. In the Euler-Lagrange model, the Navier-Stokes equations are solved for the fluid phase that is treated as a continuum whereas the discrete phase is represented and tracked as a number of elements in the form of particles, bubbles or droplets. Continuous phase and discrete phase can exchange momentum, mass and energy during the process [22, 23]. The particles are modeled and tracked in simulations through Newton's second law of motion: different forces act on every particle in a centrifugal flow field (centrifugal forces, drag forces, gravitational forces, etc.).

The volumetric proportion of discrete phase to continuous phase, however is the limiting factor of the Euler-Lagrange approach, as an increasing number of elements

requires particle-particle interaction models (Norouzi et al., 2016). The possibility of modeling and calculating the trajectories of each particle separately in the flow field becomes the major advantage of a Euler-Lagrange approach [25] in this study. Bovine milk can have, approx. 1kg sediment per 10,000 liters [26]. This proportion between the two phases represents an ideal structure for sparse discrete phase modeling in a CFD-DEM environment or in this study, ANSYS® Fluent® v19.1. Due to the relatively low counts of leukocytes in bovine milk, the particle-particle interactions in CFD-DEM modeler have been deactivated. The two-way turbulence coupling, on the other hand, is required as particles actually are affected by the character of continuous medium. It is also possible to say the vice-versa as particle movement can affect back the continuous medium in particles vicinity, an aspect the two-way turbulence coupling handles by default. Another key configuration to the simulations is that as g-force is generated by means of rotation, Moving Reference Frame (MRF) modeling in ANSYS Fluent is utilized. To satisfy this condition, the 2D model representing the disk interval is extruded by 0.15mm, since MRF modeling requires a 3D domain to operate. In meshing operation, this is split into 3 equal divisions of 0.05mm thicknesses.

Mathematical Formulation of the Liquid Phase

According to problem definition investigated in this study, the N-S equation set is described for cylindrical coordinates, as the means of generating the motive for particle sedimentation originates from the rotational movement of the device, therefore the disk interval. For an incompressible, isothermal flow (density, ρ_m = const., viscosity μ = const.), with a velocity field of $\vec{u}$ = (u_z, u_r, u_θ), the N-S equations take the form given below [27];

r-component;

$$\rho_m\left(\frac{\partial u_r}{\partial t}+u_r\frac{\partial u_r}{\partial r}+\frac{u_\theta}{r}\frac{\partial u_r}{\partial \theta}-\frac{u_\theta^2}{r}+u_z\frac{\partial u_r}{\partial z}\right) = \frac{\partial P}{\partial r}+\rho_m g_r+\mu\left[\frac{1}{r}\frac{\partial}{\partial r}\left(r\frac{\partial u_r}{\partial r}\right)-\frac{u_r}{r^2} + \frac{1}{r^2}\frac{\partial^2 u_r}{\partial \theta^2}-\frac{2}{r^2}\frac{\partial^2 u_r}{\partial \theta^2}+\frac{\partial^2 u_r}{\partial z^2}\right] \quad (4)$$

z-component;

$$\rho_m\left(\frac{\partial u_z}{\partial t}+u_r\frac{\partial u_z}{\partial r}+\frac{u_\theta}{r}\frac{\partial u_z}{\partial \theta}+u_z\frac{\partial u_z}{\partial z}\right) = \frac{\partial P}{\partial z}+\rho_m g_z+\mu\left[\frac{1}{r}\frac{\partial}{\partial r}\left(r\frac{\partial u_z}{\partial r}\right)+ + \frac{1}{r^2}\frac{\partial^2 u_{z'}}{\partial \theta^2}+\frac{\partial^2 u_z}{\partial z^2}\right] \quad (5)$$

θ-component;

$$\rho_m\left(\frac{\partial u_\theta}{\partial t}+u_r\frac{\partial u_\theta}{\partial r}+\frac{u_\theta}{r}\frac{\partial u_\theta}{\partial \theta}-\frac{u_r u_\theta}{r}+u_z\frac{\partial u_\theta}{\partial z}\right) = -\frac{1}{r}\frac{\partial P}{\partial \theta}+\rho_m g_\theta+\mu\left[\frac{1}{r}\frac{\partial}{\partial r}\left(r\frac{\partial u_\theta}{\partial r}\right)-\frac{u_\theta}{r^2} + \frac{1}{r^2}\frac{\partial^2 u_\theta}{\partial \theta^2}-\frac{2}{r^2}\frac{\partial u_r}{\partial \theta}+\frac{\partial^2 u_\theta}{\partial z^2}\right] \quad (6)$$

The problem of whether to utilize a Reynolds Averaged Navier-Stokes (RANS) model, i.e. a turbulent flow regulation is approached by calculating the Reynolds numbers for the relative velocity magnitudes at the channel inlet. The velocities were calculated through the previously stated CFD model (see Table 1 above), to be 5.531 m/s, 3.629 m/s and 1.858 m/s at angular rates of 11,550rpm, 7,700rpm and 3,850rpm, respectively. With a hydraulic diameter of 3.7×10^{-5} m for a rectangular cross-sectioned channel as in the current study, this provides a Reynolds number for the highest inlet velocity as calculated below;

$$\mathrm{Re}=\frac{\rho\vec{u}D_h}{\mu}=\frac{1035\frac{kg}{m^3}\times5.531\frac{m}{s}\times3.7\times10^{-5}m}{0.003003\ Pa\cdot s}=70.6$$

which clearly indicates laminar flow. Similarly, for 7700 rpm and 3850 rpm channel rates, Reynolds numbers are calculated to be 46.3 and 23.7, respectively. Based on this preliminary investigation, conducting the core study through laminar flow regulation in CFD software is decided. This is also justifying as the Stokes' law is known to valid only with laminar flows [28]. The outcome of this approach is also discussed with the results of calculated Reynolds numbers along the channel.

Mathematical Formulation of the Particles

The approach assumed in this study handles the discrete particles as spheres. Although custom shaped geometries are also possible by connecting and coalescing varying number of spherical elements [29], the significant computational effort this process demands often puts forward the limiting factor of this approach. Relatively low density of solid particles inside raw milk structure made modeling spherical particles feasible for DEM mainframe in the current study.

Force balance on the particle confined in a continuous medium where $\vec{F}$ is an additional acceleration term.

$$\frac{d\vec{u}_p}{dt}=F_D(\vec{u}-\vec{u}_p)+\frac{g(\rho_p-\rho_m)}{\rho_p}=\vec{F} \quad (7)$$

Sigma J Eng Nat Sci, Vol. 40, No. 2, pp. 356–369, June, 2022

The drag force per unit particle mass is,

$$F_D = \frac{18\mu}{\rho_p d_p^2}\frac{C_D Re}{24} \tag{8}$$

where, $\vec{u}$ and $\vec{u}_p$ are the velocity of continuous medium and particle, respectively, μ is the dynamic viscosity of the fluid, ρ_m and ρ_p are the densities of the medium and particle, and d_p is the particle diameter. Relative Reynolds number;

$$Re \equiv \frac{\rho d_p |\vec{u}_p - \vec{u}|}{\mu} \tag{9}$$

The additional force term, $\vec{F}$, in Eqn. 7 also includes forces on particles that originate from the rotation of the reference frame, i.e. when a Moving Reference Frame (MRF) is applied. For rotation defined about the z axis, as in our study, the forces on the particles in the remaining cylindrical directions can be written as in Eqn.'s 10 and 11.

$$\left(1-\frac{\rho_m}{\rho_p}\right)N^2 r + 2N\left(u_p - \frac{\rho_m}{\rho_p}u_r\right) \tag{10}$$

where u_p and u_r are the particle and fluid velocities in the cylindrical coordinates, N is the RPM, and;

$$\left(1-\frac{\rho_m}{\rho_p}\right)N^2 z + 2N\left(u_p - \frac{\rho_m}{\rho_p}u_z\right) \tag{11}$$

where u_p and u_z are the particle and fluid velocities in the cylindrical coordinates.

Mesh Structure

Having the number of subsequent disks reduced to a single one and confining the flow field to this alternative domain made a proper adjustment of element sizing/solution time trade-off possible. To generate a properly conditioned mesh with optimum number of elements, the disk geometry is abbreviated only to contain the conical slope, and the horizontal rabbet. Element size on the geometry is limited to 0.03mm, where the channel width is 0.25mm. Needless to say, reducing the element size indefinitely, hence increasing the total number of elements may increase the convergence ability of an analysis, while inevitably compromising the time required for solution. In a study based solely on a computational solution of an engineering system instead of experimental validation, a high convergence factor is rather necessary [30, 31]. Therefore, a verification case, with six orders of magnitude drop in solution residuals of N-S and continuity parameters were targeted. After a set of preliminary runs of the simulation with different mesh characteristics, the structure of 3,580,612 elements with 1,126,091 nodes was observed to satisfy this requirement.

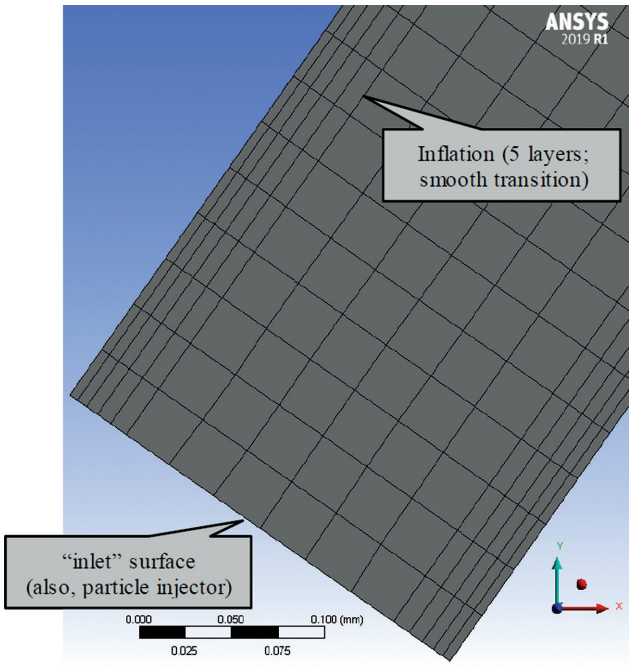

Figure 4. Mesh structure optimized for convergence-time consumption motive. Tetrahedrons are preferred for better surface refinement.

The resulting grid is comprised of fully mapped, all-hexagonal elements. A uniform body sizing function is implemented on the model to obtain proper mesh characteristics. Assuming the average inlet velocity of 3.5 m/s as a means of judging the inflation characteristic to be applied, the first layer thickness is calculated to be 0.005mm to yield a y+ of 100 (Fig 4). Although the flow regime is expected to show a laminar character due to Reynolds numbers calculated above, employing an inflated structure compensates for the no-slip boundary condition at walls, allowing the solution to better capture the velocity development near boundaries, also improving the converging ability.

Boundary Conditions

The boundary conditions are determined regarding the MRF model characteristics to represent the angular movement of disk interval. Considered as a single-input-single-output system, the disk interval only has two openings, named 'inlet' and 'outlet'. Domain motion with constant angular velocity is assumed since the preferred method based on problem definition is MRF modeling. Particles along with the continuous fluid are introduced from the inlet for conventional settling investigation and from outlet to find out shortest settling distances elapsed. MRF and DEM characteristics of all faces on the model geometry are summarized in Table 3. Particle interaction with continuous phase is allowed and DEM sources are updated every flow iteration. Solver uses unsteady particle tracking for

Table 2. Cut-off particle diameters for increasing bowl rates.

Boundary	Value	MRF Behavior	DEM Behavior
inlet (Velocity Inlet)	1.86 m/s @ 3850 rpm 3.63 m/s @ 7700 rpm 5.53 m/s @ 11550 rpm	N/A	Trap
outlet (Pressure Outlet)	2.17 atm (Ekin, 2019)	N/A	Escape
wall (Other Surfaces)	No-slip Wall	Rotational, Rel. to Adj. Cell Zone	Reflect

discrete particles, but the continuous phase is solved in a steady scheme as all the simulations are conducted for steady operation of the machine.

Simulation Procedure

Since the DEM simulation is built on the two-way interaction of phases, a pseudo-transient case is considered where particle iterations are handled in a transient way while continuous medium is treated in a steady scheme. This way, the Eulerian phase is assumed to be steady-state and particle progress is treated as time-dependent. In order to properly represent the particle behavior during the simulation, the DEM time steps must be determined accordingly. The best resolution between particle and continuous medium advancements is when the particle fates are calculated properly within every continuous medium iteration (no 'incomplete' particles to be present in flow domain). To satisfy this necessity and to better represent the particle behavior in the elements adjacent to the 'inlet' boundary, a 10^{-7}s particle time step is assumed. Convergence characteristics of laminar model and successful particle trajectory generation prove that this time step assessment is valid (see Fig. 5 below).

In this study the 'SIMPLE' algorithm within the Fluent Solver is utilized to calculate the governing equations of the Eulerian phase model equations. As stated previously, since the particles confined in the continuous medium are considered sparse, particle-particle interactions (DEM collision) are not activated. Tracking scheme for the Discrete Phase Model is automated with trapezoidal high order scheme and implicit low-order scheme. Throughout the numerical solutions, a tracking file for every cut-off size particle is generated.

Number of particles injected at each run of simulations can be determined through various methods. In the current study, 'surface injection' is selected to investigate whether particle behavior is affected by the injection location as well as other boundary conditions and DEM parameters outlined in Tables 4. In this convention, the number of injected particles is determined directly by the number of elements on the surface. In the current mesh structure, this number is set to 48, hence 48 particles to be tracked. In actual applications, based on the nature of particle-laden flow, the number of particles introduced into the sedimentation volume per unit time may differ. In this study, the number given is deemed appropriate as it represents injection of particles from 48 different locations along the 'inlet' boundary, at a length of 0.25mm. Also, no relative velocity to the particles is defined since the particles are introduced alongside the continuous medium in actual process and not injected separately.

Table 3. Cut-off particle diameters for increasing bowl rates.

DEM Parameter	Value
Max Number of Steps	10^9 (max. allowed)
Length Scale	10^{-5} m
Particle Time Step	10^{-7} s
Accuracy Tolerance	10^{-5}
Max Refinements	20
Tracking Scheme	Trapezoidal (High Order Scheme) Implicit (Low Order Scheme)
Particle Physical Model	Spherical
Surface Inj.	From 'inlet' Boundary
Number of Particles Injected	48 (per total number of elements on the boundary)

Two distinct set of injections are considered to investigate the phenomenon thoroughly: in the first set of simulations, injection of particles is conducted separately via 'surface' definition where the inlet of disk interval is also selected to be the injection surface where 48 particles are introduced to the volume. For the second set of simulations, particles at a range of 0.01μ and 12μm, also including the three cut-off diameters are injected in separate runs to investigate diameter-sedimentation relationship in isolated conditions, i.e. constant angular velocity, inlet velocity etc. The DEM parameters are selected to provide the best possible particle tracing for both scenarios of particle injection

Sigma J Eng Nat Sci, Vol. 40, No. 2, pp. 356–369, June, 2022

without the expense of acceptable solver time (Table 4). All of the calculations were finished within a month using a 64-bit computer with Intel Core i7-8700 6-core CPU supported by 32.0GB of RAM.

RESULTS AND DISCUSSION

Fig.'s 5 and 6 represent the velocity distributions in the inclined channel that is the disk interval, through the elements located in the direction normal to the flow direction. In the channel cross-section (Fig.5), the relative velocity drops to zero in the vicinity of walls, due to no-slip boundary condition. This is better observed thanks to inflation application near wall boundaries. Flow develops quickly into a uniform velocity profile in the channel cross-section. This implies that the assumption the flow is uniform through a disk-stack can be justified as well as the assumption that the total mass flow rate is divided into nearly equal partitions through many disks comprising the disk-stack. Fig.6 displays a contour-graph alternative to Fig. 5, as near the wall boundaries the relative velocity of the continuous medium gradually drops to zero on both sides.

Relative velocity distribution along the channel length can be seen on Fig. 7. It is important to underline that the velocities are extracted relative to the adjacent cell zone, that is the flow domain. Absolute velocities are not considered this point as in this case the magnitudes are determined mainly by the rotational movement of the domain and not the inlet velocities at the boundary. Therefore, both in velocity graphs and Reynolds number distributions, relative velocities are utilized. From that perspective, the maximum velocities are observed at the inlet boundary at 11,550rpm to be 14 m/s. Relative velocity magnitudes tend to drop as resistance to flow is ever-present due to the g-force alongside the counterpressure applied on the outlet boundary of the domain.

It is important to recognize that, Reynolds number is calculated element (cell) based in ANSYS Fluent. That is, the hydraulic diameter is calculated for each and every cell along the given path or region. Also, the Cell Reynolds Number is calculated for the absolute velocities only (ANSYS Inc., 2010). As this approach becomes inconvenient with the rest of the simulation procedure adopted in this study, the Reynolds numbers are calculated via relative velocities and the hydraulic diameter described previously. The resulting diagram of Reynolds number distributions along the flow field are given on Fig. 8, indicating a laminar flow along the channel, despite the fact that centrifugal forces exceeding 12,000g (at 11550rpm) are exerted on the fluid, hence the particles. This character of flow in terms of flow conditioning gives the centrifugal disk settler its cutting edge, also justifying the convenience of utilizing the laminar model.

Through pressure distribution, due to the insight it provides towards the required strength to be satisfied in the mechanical structure of the centrifuge, is a significant output from the investigation. Here, the relevant pressure parameter is the dynamic pressure, since the entire set of

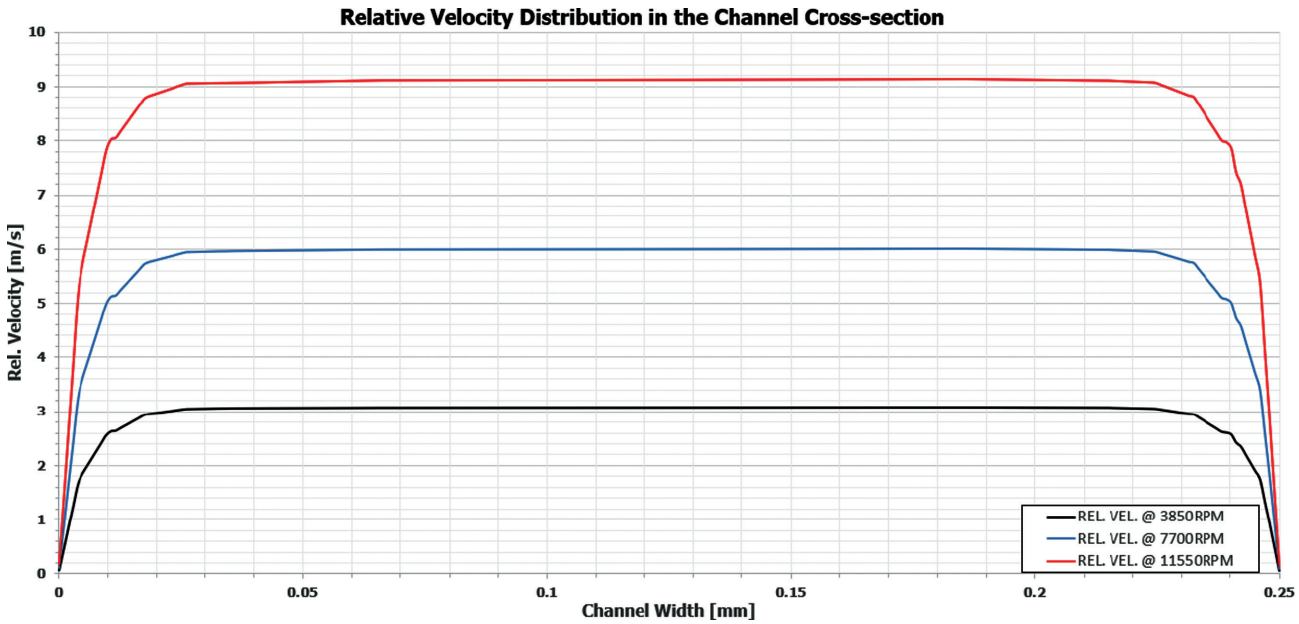

Figure 5. Relative velocity across the width (0.25mm) of the channel displays a uniform profile, despite the presence of violent centrifugal forces.

simulations are commenced for a moving fluid in a rotational domain, hence the MRF modeling. Although not a direct point of interest in this study, the counter-pressure applied to set the retention time also plays a certain role in the results presented in the Fig. 9.

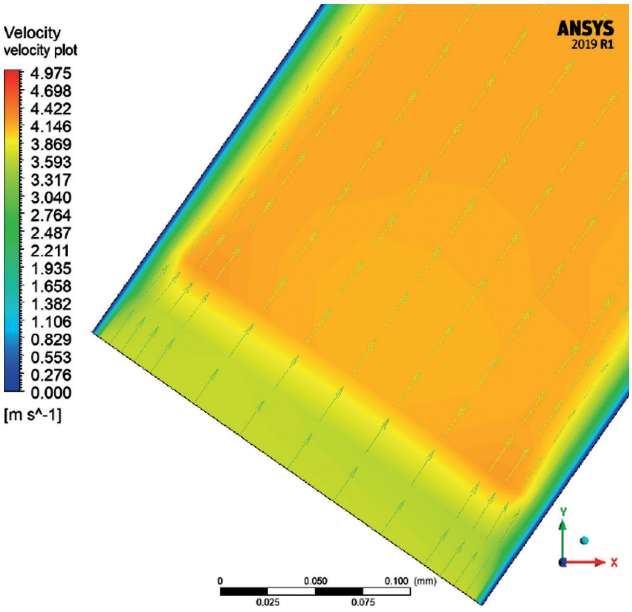

Figure 6. Relative velocity across the width (0.25mm) of the channel displays a uniform profile, despite the presence of violent centrifugal forces.

The increment in the pressure levels near the inlet boundary becomes more violent in 7700rpm – 11550rpm transition when compared to 3850rpm – 7700rpm transition in Fig. 9. This change actually indicates the reasoning behind the angular velocity choice when a particular process is considered: required mass flow rate limits the dimensions of the machine (through bowl volume that is constant), therefore the dimensions of the disk-stack. On the trade-off, the disk-stack geometry, along with the angular velocity determines the limit particle size that can be sedimented through the channel. When certain levels of pressure are considered, it becomes obvious that for a particular type of sediment, the disk-stack is 'shrunk' in size to compensate for the extreme pressure levels. Although the smooth decrease in pressure through the channel represents an attraction for particles to move along the current, it is necessary to remark the effect of the centripetal forces acting on particles.

As stated previously, due to the intricacy of the procedure of taking samples or measurements out of a single disk interval, the main mechanism to justify the above results concerning the flow field was verification. In Fig. 10, as a residual monitor from the simulations conducted through the study (specifically, for 7700rpm case), six orders of magnitude drop, as proposed, can be seen for each laminar flow parameter solved by the software. This magnitude drop is expected, as one reason for simplifying the entire disk-stack centrifuge into a single-disk interval was to better modify the mesh quality (also the inflation application) to capture

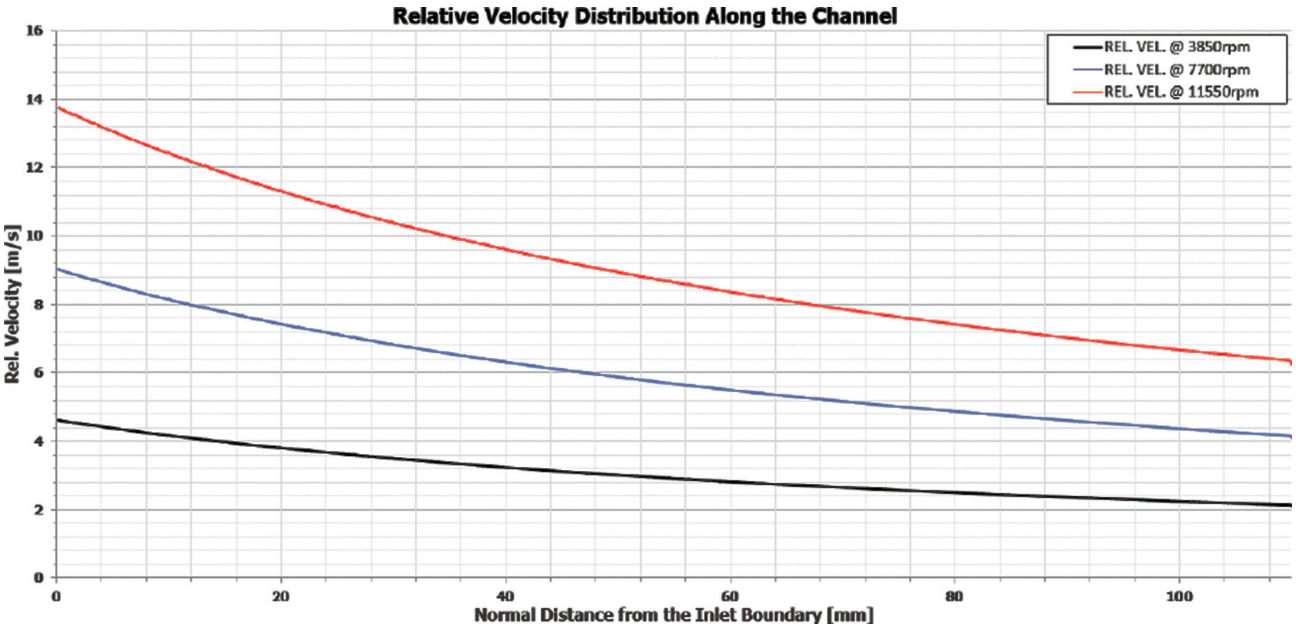

Figure 7. Relative velocity across the width (0.25mm) of the channel displays a uniform profile, despite the presence of violent centrifugal forces.

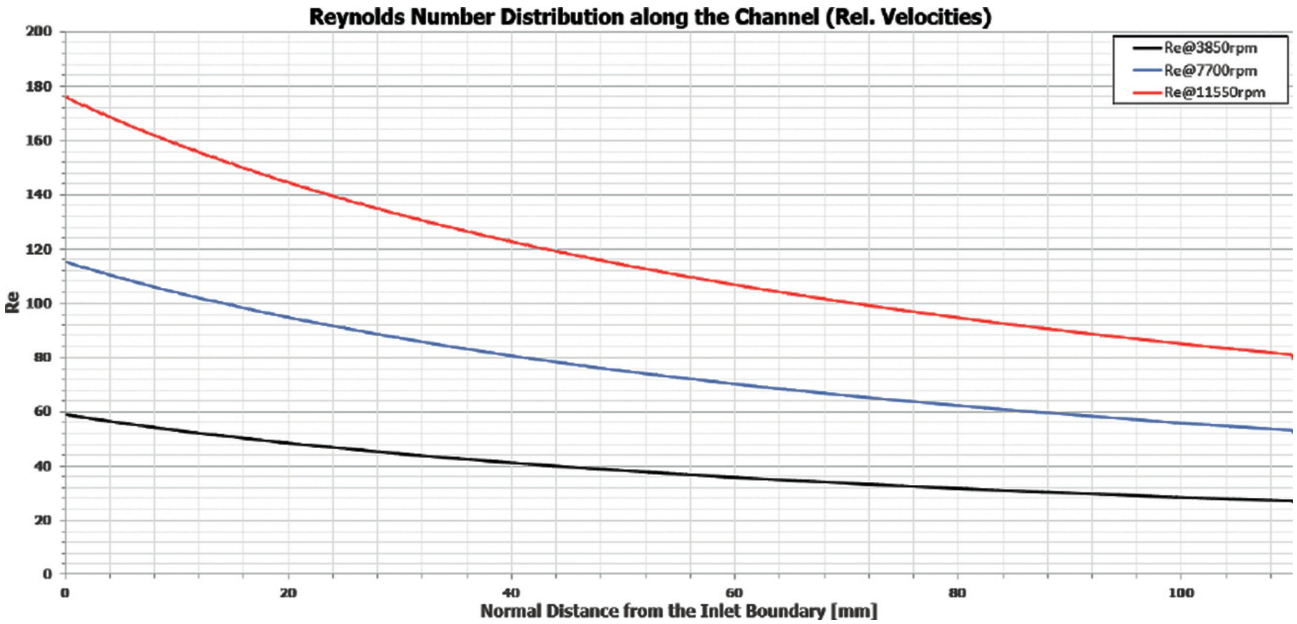

Figure 8. A certain decrease in Re number after injection boundary is observed due to channel geometry.

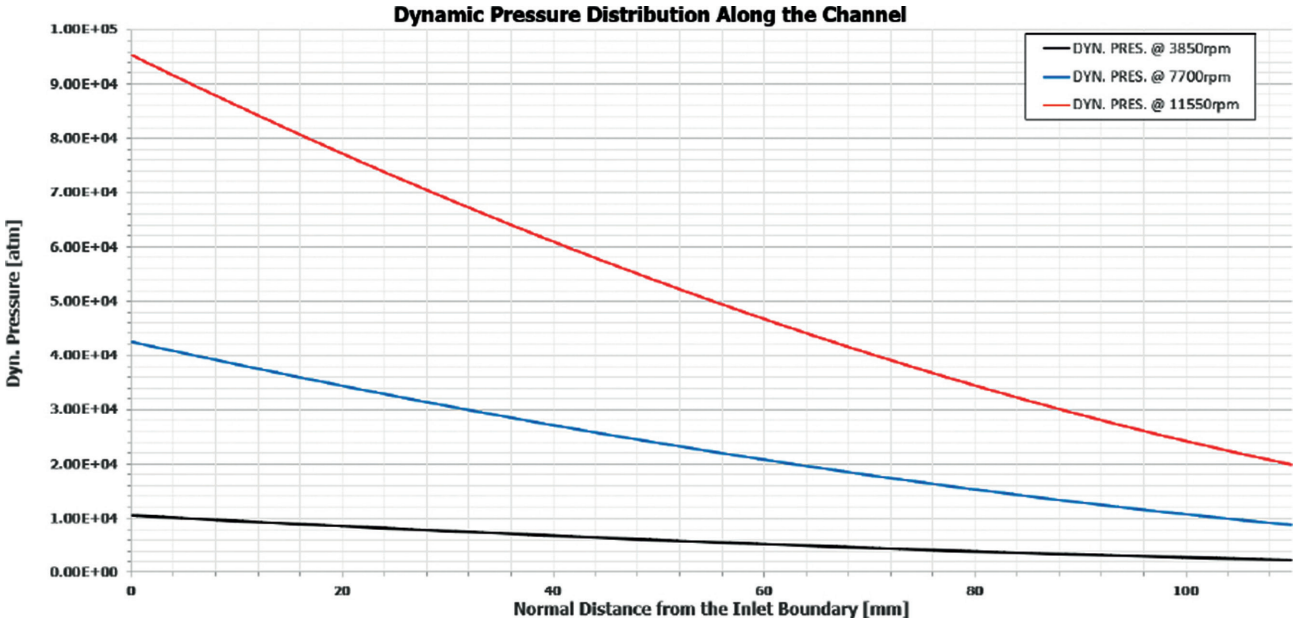

Figure 9. The drop in pressure along the channel axis is also a correspondence to the disturbances in velocity.

the flow and particle parameters at higher precision without compromising the solver-time efficiency.

Despite the typical disk-stack utilized in the commercial device this study is based upon provides a 110mm channel length (relatively long in proportion to the channel width, 0.25mm), the particle settling usually occurs near the inlet boundary (Fig. 11) as the simulations suggested. Here, a particle time-step value of 10^(−5) s is adopted at pseudo-transient analysis. The particle track demonstration shows the exact number of discrete particles to get sedimented (on the 'inlet' boundary) or escaped to the clarified phase (through the 'outlet' boundary). Sedimentation results in terms of particle fates, regarding the three different injections are summarized on Table 5.

Particles fail to reach the clean outlet boundary, in the commercial side of the application, are also considered as settled, which corresponds to the way the somatic cell counting methods applied to samples collected from the actual process. The phenomenon is also observed during the simulations, regardless of the inlet BC's but due to very small particle time-step size preferred. Since the fluid flow displays a laminar character and trajectories are not distracted by the eddy currents within the channel domain, the particles still tracked after 30,000 time-steps are assumed to be escaped without sedimentation (Fig.s 11 and 12).

Table 5 shows the detailed particle fates for independent injections of cut-off size particles at corresponding channel rates. As stated previously, decreasing the angular velocity of the channel results in larger cut-off size diameters. Judging from the tabular data (that supports the depiction of tracks in Fig. 11) g-force, as a process parameter, is the foremost motive of the sedimentation, with the largest Ambler cut-off size is sedimented at only 22.9%, whereas the smallest diameter at a 66.7%. The best result is observed at 7700rpm and its cut-off size of 3.131μm which verifies the optimum (or design) point.

As an alternative to separate injection scheme to obtain a reliable basis for centrifuging implementation through CFD-DEM, also a simultaneous particle injection/tracking case is developed in the context of this study. Inferencing the response of above- and below-cut-off size diameters for a distinct channel rate was the aim of this second simulation case. Injections were made in the same fashion, i.e., from the inlet boundary. The particle trajectories aside (see Fig. 12 below), it is apparent from the Table 6 that injecting a particle size that is larger than the corresponding cut-off size for a specific angular velocity is not the guarantee of that larger size will be sedimented at greater percentages.

When the detailed particle fates of the simultaneous injections are investigated in Table 6, slightly different results in particle sedimentation are observed. Judging

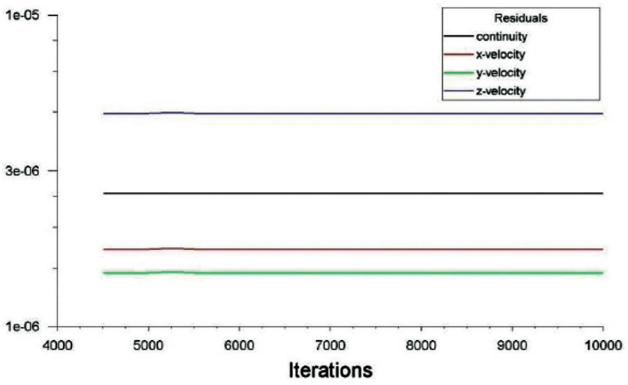

Figure 10. Laminar solution of continuous flow demonstrates a six-figure magnitude drop for each angular velocity of the channel.

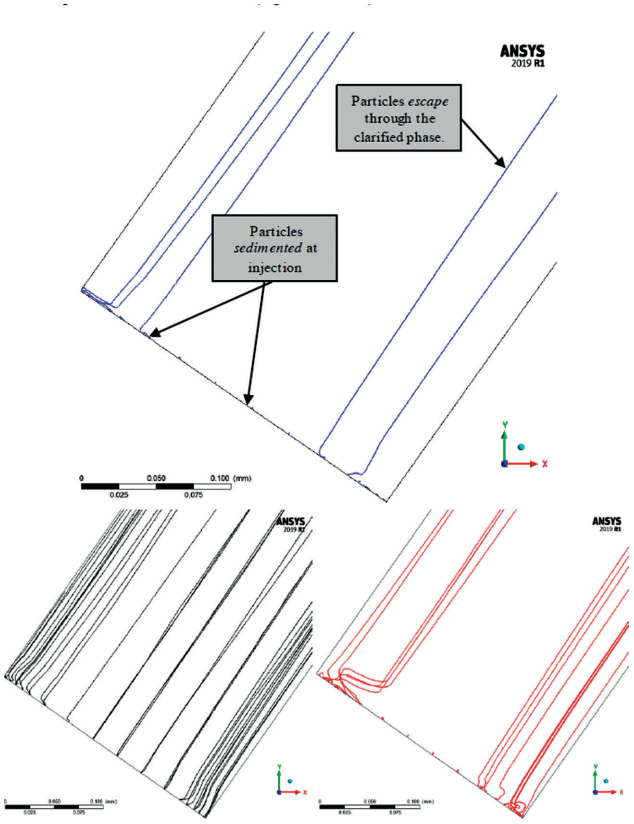

Figure 11. Judging from the cut-off size, the settling behavior for optimum channel angular velocity at 7700rpm (above) displays radical differences when compared to 3850rpm (left) and 11550rpm alternatives (right).

Table 4. Particle fates for average relative centrifugal forces after 30,000 particle time-steps at 10^(-5) s particle time-step size.

Channel Rate [rpm]	Rel. Centrifugal Force [g]	Inlet Velocity [m/s]	Diameter (cut-off) [μm]	Sedimented
3,850	1,359	1.86	6.259	22.9%
7,700	5,435	3.63	3.131	**87.5%**
11,550	12,228	5.53	2.086	66.7%

Sigma J Eng Nat Sci, Vol. 40, No. 2, pp. 356–369, June, 2022

from the tendency, it is convenient to say that the Stokes' law can be translated into CFD-DEM at a certain extent. On the other hand, it is evident that both particle sizes lower and higher than that of Ambler [9] cut-off size calculation give sedimentation ratios significantly larger than 50%.

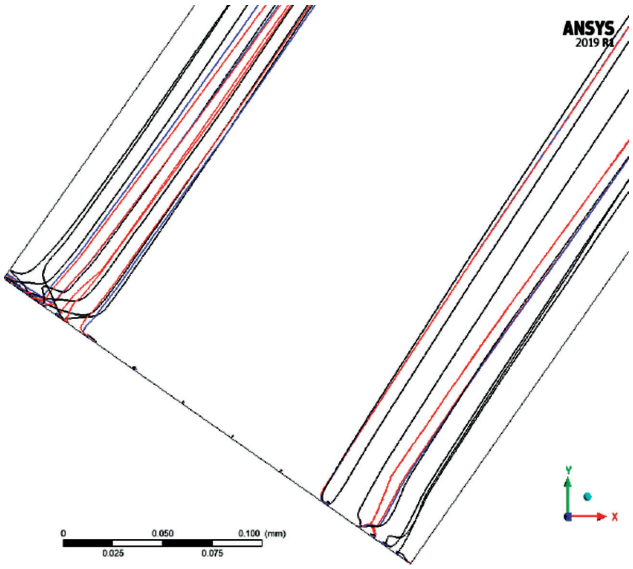

Figure 12. Simultaneous injections of above- and below-cut-off size particles at 7700rpm display alternative trajectories and fates, when compared to separate injection runs.

Finally, simulations based on a range of particles, including the three cut-off sizes mentioned above, is implemented to observe particle sedimentation efficiencies when the angular velocity of the channel is fixed (Fig. 13). The range of particle sizes is derived from the article by Zlotnik [16] for somatic cells, with the lower end of the range reduced down to 0.01μm to represent an extreme. The diagram shows a peak sedimentation efficiency at rather lower ends of size range, i.e., 2~4μm interval where the maximum efficiency is again reached by 7700rpm at its calculated cut-off diameter, 3.131μm. It is apparent from the Fig. 13 that as the diameter increases, the buoyancy force acting on the particle overwhelms the centrifugal settling force, therefore the escape to the clarified phase.

CONCLUSION

In-depth simulations performed during this study suggest a relationship between particle sedimentation

Table 5. Particle fates at 7700rpm, after 30,000 timesteps, with 10^{-5} s particle time-step size.

Angular Velocity [rpm]	Rel. Centrifugal Force [g]	Inlet Velocity [m/s]	Critical Diameter [μm]	Sedimented
			6.259	70.83%
7,700	5,434.80	3.63	3.131	**87.5%**
			2.086	81.25%

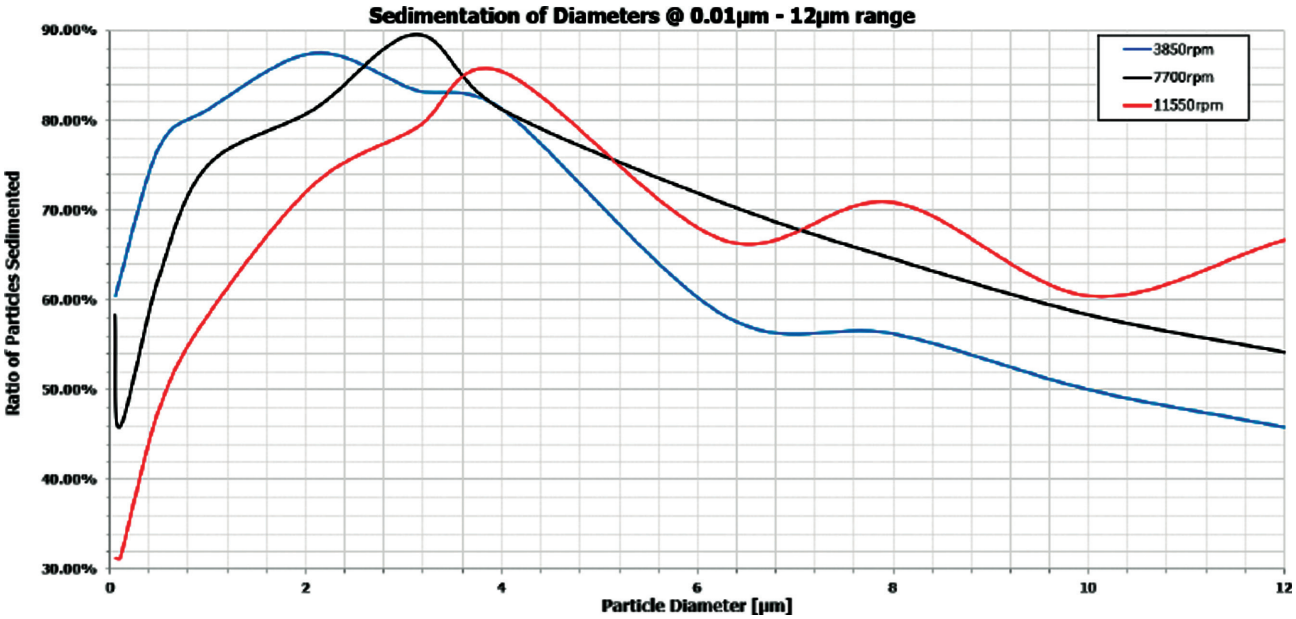

Figure 13. For the same size range of particles, every channel rate (therefore g-force level) suggests a size at which the peak ratios of sedimentation are realized.

and process parameters like centrifugal forces, pressure gradients and buoyancy forces acting on particles due to continuous fluid flow. The effects of flow modeling through the inclined disk geometry are best observed when velocity and pressure distributions in through and cross sections of the channel are considered. This implementation is also important since in any commercial machine of this specific type, the disk-stack behavior is a black-box operation where data is only collected from either inlet or the exit line of the machinery. By observing the flow field in a single-disk interval through computational methods, a more convenient assessment has been realized.

Critical particle diameter that can be sedimented out of the inclined channel is acutely connected to the angular velocity. The set of simulations conducted in this study also displayed a parallel view to theoretical adaptations of Stokes' Law into centrifugal sedimentation processes. However, the main goal of a typical mechanical separation process is seldom about eliminating the lower-limit particle size. Therefore, theoretical cut-off size should correspond to the average particle size the particle-laden fluid offers, followed by a careful inspection and verification through CFD-DEM. In this direction, once the process and particle-laden medium properties are set, it is possible to simulate, through the Stokes' law, for the optimum g-force required to sediment the target particle size (hence, the cut-size) at highest ratios.

NOMENCLATURE

P:	Pressure
$\vec{u}$:	Velocity Field for cylindrical coord.
u_z, u_r, u_θ:	Cont. medium velocity components
g_r, g_z, g_θ:	Gravitational components
r:	Radial distance to the axis of revolution
Re:	Relative Reynolds number
ρ_m:	Density of continuous medium
μ:	Dynamic viscosity
Q:	Throughput rate
ω, Ω:	Angular velocity
N:	Revolutions per minute
n:	Number of Disks
d_p:	Particle diameter
u_p:	Particle velocity
ρ_p:	Density of discrete particles
ϑ:	Stokes' Terminal Velocity
F_g:	Gravitational force (on the particle)
F_b:	Buoyancy Force (on the particle)
F_d:	Drag Force (on the particle)

ACKNOWLEDGEMENTS

The authors would like to thank HAUS Centrifuge Technologies for their elaborate 3D models and fieldwork.

REFERENCES

[1] Records A, Sutherland, K. Decanter Theory: Decanter Centrifuge Handbook. Oxford: Elsevier Science Ltd.; 2007.

[2] Triebel H, Birnie GD, Rickwood D. Centrifugal Separations in Molecular and Cell Biology. London, Butterworths & Co. Publishers Ltd.; 2007.

[3] Spreer E. Milk and Dairy Product Technology. Oxfordshire: Taylor and Francis; 2017.

[4] Leung WWF. Centrifugal Separations in Biotechnology. 1st ed. Amsterdam: Elsevier; 2007. [CrossRef]

[5] Shekhawat LK, Sarkar J, Gupta R, Hadpe S, Rathore AS. Application of CFD in Bioprocessing: Separation of mammalian cells using disc stack centrifuge during production of biotherapeutics. J Biotechnol 2018;267:1–11. [CrossRef]

[6] Janoske U, Piesche M. Numerical simulation of the fluid flow and the separation behaviour in a disc stack centrifuge. High Performance Comput Sci Eng 1999;98:261–268. [CrossRef]

[7] Tsuji Y, Tanaka T, Ishida T. Lagrangian numerical simulation of plug flow of cohesionless particles in a horizontal pipe. Powder Technol 1992;71:239–250. [CrossRef]

[8] Ambler CM. The theory of scaling up laboratory data for the sedimentation type centrifuge. J Biochem Microbiol Technol Eng 1959;1:185–205. [CrossRef]

[9] Ekin O, Çerçi Y. A discrete element modeling investigation of the centrifugal separation process of bovine milk somatic cells. Sigma J Eng Nat Sci 2020;37:1477–1492.

[10] van der Linden JP. Liquid-Liquid Separation in Disc-stack Centrifuges. [Doctoral Thesis Dissertation], Delft University of Technology, 1987.

[11] Kilara A, Chandan RC. Dairy Ingredients for Food Processing. New Jersey: Wiley-Blackwell; 2011. [CrossRef]

[12] Vesilind PA. The Rosin-Rammler particle size distribution. Resource Recovery and Conservation 1980;5:275–277. [CrossRef]

[13] Li N, Richoux R, Boutinaud M, Martin P, Gagnaire V. Role of somatic cells on dairy processes and products: A review. Dairy Sci Technol 2014;94:517–538. [CrossRef]

[14] Zlotnik I. Types of cells present in Cow's milk. J Compr Pathol Ther 1947;57:196–208. [CrossRef]

[15] Zipursky A, Bow E, Seshadri RS, Brown EJ. Leukocyte density and volume in normal subjects and in patients with acute lymphoblastic leukemia. Blood 1976;48: 361–371. [CrossRef]

[16] Cundall PA, Strack ODL. A discrete numerical model for granular assemblies, Géotechnique 1979;29: 46–65. [CrossRef]

[17] Tsuji Y, Kawaguchi T, Tanaka T. Discrete particle simulation of two-dimensional fluidized bed. Powder Technol 1993;77:79–87. [CrossRef]
[18] Cleary PW, Hilton JE, Sinnott MD. Modelling of industrial particle and multiphase flows. Powder Technol 2017;314:232–252. [CrossRef]
[19] Harting J, Frijters S, Ramaioli M, Robinson M, Wolf, DE, Luding S. Recent advances in the simulation of particle-laden flows. Eur Phys J Spec Top 2014;223:2253–2267. [CrossRef]
[20] Kartushinsky A, Tisler S, Oliveira JLG, van der Geld CWM. Eulerian-Eulerian modelling of particle-laden two-phase flow. Powder Technol 2016;301:999–1007. [CrossRef]
[21] Zhong W, Yu A, Liu X, Tong Z, Zhang H. DEM/CFD-DEM modelling of non-spherical particulate systems: theoretical developments and applications. Powder Technol 2016;302:108–152. [CrossRef]
[22] Zeng D, Zhang E, Ding Y, Yi Y, Xian Q, Yao G, et al, Investigation of erosion behaviors of sulfur-particle-laden gas flow in an elbow via a CFD-DEM coupling method. Powder Technol 2018;329:115–128. [CrossRef]
[23] Shiozawa S, McClure M. Simulation of proppant transport with gravitational settling and fracture closure in a three-dimensional hydraulic fracturing simulator. J Pet Sci Eng 2016;138:298–314. [CrossRef]
[24] Norouzi HR, Zarghami R, Sotudeh-Gharebagh R, Mostoufi N. Coupled CFD-DEM Modeling: Formulation, Implementation and Application to Multiphase Flows. New Jersey: John Wiley & Sons; 2016. [CrossRef]
[25] Capecelatro J., Desjardins, O., A Euler–Lagrange strategy for simulating particle-laden flows. J Comput Phys 2013;238:1–31. [CrossRef]
[26] Walstra P, Wouters JTM, Geurts TJ. Dairy Technology: Principles of Milk Properties and Processes. Boca Raton, Florida: CRC Press; 1999. [CrossRef]
[27] White F. Fluid Mechanics 4th ed. 2000, Pennysylvania: McGraw-Hill International Editions; 2000.
[28] Minjun M, Julius A, Cheang K. Microbiorobotics Biologically Inspired Microscale Robotic Systems. Cambridge: Elsevier; 2017.
[29] Guo Y, Yang Y, Yu X. Influence of particle shape on the erodibility of non-cohesive soil: Insights from coupled CFD–DEM simulations. Particuology 2018,39:12–24. [CrossRef]
[30] Stern F, Wilson RV, Coleman HW, Paterson EG. Verification and Validation of CFD Simulations, 1999, Iowa Institute of Hydraulic Research, College of Engineering, The University of Iowa, Iowa City IA. 2001 Fluids Engineering Division Summer Meeting May 29 - June 1, 2001, New Orleans, Louisiana, 2001.
[31] Versteeg KH, Malalasekera W. An Introduction to Computational Fluid Dynamics. New York: Pearson Education Limited: 2017.